A NEW KAOLIN DEPOSIT IN WESTERN AFRICA: MINERALOGICAL AND COMPOSITIONAL FEATURES OF KAOLINITE FROM CALUQUEMBE (ANGOLA)

ESPERANÇA TAULER[1], JINGYAO XU[1*], MARC CAMPENY [1,2], SANDRA AMORES[1], JOAN CARLES MELGAREJO[1], SALVADOR MARTINEZ[1] AND ANTONIO O. GONÇALVES[3]

[1] Departament de Mineralogia, Petrologia i Geologia Aplicada, Facultat de Ciències de la Terra, Universitat de Barcelona, Barcelona, Spain

[2] Departament de Mineralogia, Museu de Ciències Naturals de Barcelona, Barcelona, Spain

[3] Departamento de Geologia, Universidade Agostinho Neto, Luanda, Angola

* e-mail: jingyao.xu@ub.edu

Abstract - Large kaolin deposits developed by weathering on Precambrian granitic rocks have been discovered in the Caluquembe area, Huíla province, Angola. To determine accuracy of analysis and to evaluate the samples kaolinite grade, it was used full profile Rietveld refinement by X-Ray Powder Diffraction (XRPD) and Gravimetric Thermal Analysis (TGA). Caluquembe kaolin is mainly comprised of kaolinite (44 to 93 wt. %), quartz (0 to 23 wt. %) and feldspar (4 to 14 wt. %). AGFI Crystallinity Index, calculated by XRPD profile refinement, indicates low and medium defect kaolinite. Kaolinite particles show a platy habit and they are stacked together forming 'booklets' or radial aggregates, also occurring as fine anhedral particles in a finer-grained mass. Muscovite-kaolinite intergrowths have also been found. Whole-rock chemical composition was analyzed, including major, trace, and Rare Earth Elements (REE). Chondrite and Upper Continental Crust normalized REE patterns show the same tendency for all samples, with a significant enrichment in Light Rare Earth Elements (LREE). Mineralogical and compositional features of the Caluquembe kaolin indicate that it is a suitable material in the manufacture of structural products, such as bricks, pavers and roofing tiles. In addition, REE significant contents of the Caluquembe kaolin can be considered as a potential future target of mining exploration.

Key Words: Caluquembe, Angola, kaolinite, AGFI, REE.

INTRODUCTION

Kaolinite $Al_2Si_2O_5(OH)_4$ is a clay mineral, structurally classified as 1:1 layer type, with a crystalline structure comprised of tetrahedral and octahedral sheets (Young and Hewat, 1988; Moore and Reynolds, 1997; Bish, 1993). It belongs to the spatial group $C\bar{1}$ with a= 5.154 Å, b= 8.942 Å, c= 7.402 Å, α= 91.69°, ß= 104.61° and ɣ=89.92° (Bish, 1993).

Kaolinite is classified within the kaolin subgroup, which also includes other minerals such as dickite, nacrite and a hydrated form of halloysite (Guggenheim *et al*., 2006). Structural differences between these mineral phases are based on their interlayer shift and the location of the octahedral vacancy in successive layers (Bailey, 1980).

Kaolinite is a valuable and versatile industrial mineral with classical applications in the production of bricks, ceramics, paint coatings, paper, and plastic. It also has relatively new applications in catalysis and organic reactivity as well as in the pharmaceutical industry, where it is used in the design of clay-polymer nanocomposites and films (Heckroodt, 1991; Murray, 1999c; Murray, 2000; Detellier and Schoonheydt, 2014; Phipps, 2014; Pruett, 2016; Dedzo and Detellier, 2016; Nguie *et al*., 2016; Mansa *et al*., 2017).

In 2015, world kaolinite production was around 34 million tons (Mt), mainly led by the United States, Germany, Czech Republic and China, among other countries (Flanagan, 2016).

Kaolin deposits are classified as primary, secondary, or tertiary depending on their parent lithology and corresponding alteration processes (Dill, 2016). In primary deposits, the parent lithology is a feldspar-rich magmatic rock – mainly granitic or acid

55 volcanic – and the formation of kaolinite is related to feldspar alteration due to
56 hydrothermal fluid circulation and/or the development of weathering processes
57 (Schroeder and Erickson, 2014). On the other hand, sedimentary processes generate
58 secondary deposits, mainly comprised of detrital clays (Schroeder and Erickson, 2014).
59 Tertiary deposits are generated by very low regional metamorphism developed in
60 argillaceous sediments or sands (Dill, 2016).

61 Angola has significant and large mineral resources. However, for more than
62 forty years, the Angolan independence and civil wars (1961 – 2002) prevented
63 systematic mining exploration in the country. Nowadays, known mineral resources in
64 Angola include: beryllium, clays, copper, gold, gypsum, iron, lead, lignite, manganese,
65 mica, nickel, phosphates, silver, tungsten, uranium, vanadium and zinc, among others
66 (Bermúdez-Lugo, 2014). However, diamonds are the most economically relevant
67 mineral resource in the country and account for about 5% of worldwide production.

68 In the case of kaolin, significant deposits have been documented in several
69 regions in Angola (Ekosse, 2010). Most of them are related to weathering of
70 anorthosites from the Kunene anorthositic complex, but systematic studies of these
71 kaolin deposits are still very scarce. The only significant studies were carried out by
72 Gomes *et al*. (1994) and Saviano *et al*. (2005) in the Mevaiela kaolin deposit, located
73 near the village of Quihita in SE Angola.

74 In the Caluquembe area (Huíla province, Angola), (Fig. 1) extensive kaolin
75 outcrops associated to weathering of Eburnean granitic rocks were recently
76 discovered. This study presents the most relevant mineralogical and compositional
77 features of Caluquembe kaolinite. It has been determined the kaolinite grade of the
78 deposit by processing XRPD spectra using full profile Rietveld refinement and testing

79 the accuracy of the results by TGA. This study also includes kaolin major and trace
80 elements compositions, with especial interest in the distribution of Rare Earth
81 Elements (REE), considering that a significant number of REE deposits worldwide are
82 related to weathering of granitic rocks (Nyakairu and Koeberl, 2001; Nyakairu *et al*.,
83 2001; Njoya *et al*., 2006; Bao and Zhao, 2008; Galán *et al*., 2016; Sanematsu and
84 Watanabe, 2016) or from sedimentary rocks (Kadir and Kart, 2009; Elliott *et al*., 2018).
85 The results obtained may be considered as preliminary evaluation guidelines for future
86 mining exploration of kaolin and accessory REE's in the Caluquembe area.
87
88 GEOLOGICAL SETTING
89
90 The Caluquembe area is located in the Huíla province (SW Angola),
91 approximately 180 km NE from Lubango and 570 km SE of Luanda, Angola's capital
92 (Fig.1).
93 Angola's structural framework is generally represented by the Kasai and Congo
94 cratons, which correspond to continental blocks stabilized during the Mesoproterozoic
95 orogeny (Hanson, 2003; Jelsma *et al*., 2011).
96 The southwestern part of the Congo Craton comprises the Angolan Shield
97 where the occurrence of widespread Paleoproterozoic crust – dominated by granitoids
98 – has been identified together with a limited amount of Archaean crust (de Carvalho *et*
99 *al*., 2000; McCourt *et al*., 2013) (Figure 1a).. This basement terrane is intruded by the
100 anorthositic Kunene Complex (Ashwal and Twist, 1994; Mayer *et al*., 2004), a set of
101 Mesoproterozoic red granites, and it is also unconformably overlain by supracrustal
102 sequences.

The Caluquembe region is located in one of the four broad tectonic domains that form the Angolan Shield, known as the Central Eburnean Zone (de Carvalho *et al*., 2000; Jelsma *et al*., 2011; McCourt *et al*., 2013). In this domain, paleoproterozoic granitoids are the dominant lithologies (Figure 1). However, more recent lithologies such as Eburnean granitoids linked to the Namib thermotectonic event are also found outcropping in this area (de Carvalho *et al*., 2000). The predominant lithology in the sampled Caluquembe area is the regional Chicala alkaline granite (c. 1700-1650 Ma), outcropping in association with porphyritic granites and other Eburnean granites such as the Yuabre and Quibala granites (Figure 1). Hypabyssal rocks such as dolerites, norites, and olivine basalts also occur across the region – related to anorogenic magmatism that occurred in the middle and late Proterozoic and also towards the end of the Cretaceous, during the Wealdenian reactivation of the Angolan platform (c. 130-100 Ma, Silva and Simões, 1980/1981).

Strong erosion processes were developed during the Cenozoic, accompanied by intense weathering under semi-tropical climatic conditions (Marques, 1977). The alteration of granitic rocks was directly related to the formation of kaolinite weathering profiles.

SAMPLING and METHODS

In the present work, were studied a set of 34 samples obtained in extensive weathering profiles developed on granitic rocks in the Caluquembe region (Figure 2). The studied area is around 20 km^2 and sampling was mainly focused on the available outcrops located along river margins.

The morphology and microtextural features of the studied kaolin samples were examined on polished thin sections with a Nikon Eclipse LV100 POL microscope and an ESEM Quanta 200 FEI, XTE 325/D8395 scanning electron microscope with energy dispersive X-ray spectroscopy (SEM-EDS) at the Scientific and Technological Centers of the University of Barcelona (CCiTUB) (Barcelona, Catalonia, Spain).

Particle size was measured with a Beckman Coulter LS Particle Size Analyzer. To avoid sample flocculation and consequent erroneous measure of grain size distribution, approximately 0.5 grams of dry sample were diluted in a dispersing solution of sodium polyphosphate during 15 minutes using ultrasonic bath. Before the analysis the obtained solution was agitated during 24 hours. This preparation was carried out in Department of Earth and Ocean Dynamics from the Earth Sciences Faculty of the University of Barcelona (Barcelona, Catalonia, Spain).

Microprobe analyses (EMPA) were performed over selected areas on representative polished thin sections. Analyses were carried out with a JEOL JXA-8230 at the CCiTUB. Analytical conditions were a low voltage of 20 kV (in order to excite the weaker lines K, L of certain heavy elements those can present spectral interferences), 10 nA beam current, 2 μm beam diameter and counting time of 10 seconds per element.

Kaolin samples, after dried, were crushed for X-ray Powder Diffraction (XRPD) and Thermal analyses (DTA-TGA) only using agate mortar.

XRPD data were collected with a Panalytical X'Pert PRO MPD X-ray diffractometer with monochromatized incident Cu $K_{\alpha 1}$ radiation at 45 kV and 40 mA, equipped with a PS detector with amplitude of 2.113° located at the CCiTUB. Patterns were obtained by scanning random powders from 4° to 80° (2θ) on samples crushed in

151 an agate mortar to a particle size below 40 μm or on oriented mounts. The oriented
152 clay mineral aggregates were prepared by glass slide method before separating clay
153 minerals from clasts (Moore and Reynolds, 1997). Datasets were obtained using a scan
154 time of 50 seconds at a step size of 0.017° (2θ) and variable automatic divergence slit.
155 Quantitative mineral phase analyses were obtained by full refinement profile using
156 XRPD. The software used was TOPAS V4.2 (2009).

157 Thermal analyses were carried out by simultaneous DTA-TGA, using a Netzsch
158 instrument (STA 409C model) located at the Department of Mineralogy, Petrology and
159 Applied Geology from the Earth Sciences Faculty of the University of Barcelona
160 (Barcelona, Catalonia, Spain). Analyses were carried out under a temperature range of
161 25 to 950°C, atmospheric pressure, constant flow rate of 80 mL/min, and at a heating
162 rate of 10 °C/min in an Al_2O_3 crucible. The sample amount used was approximately 80
163 mg.

164 Major, minor, and trace elements were determined at the ACTLABS Activation
165 Laboratories Ltd., (Ancaster, Ontario, Canada) with the analytical package ‘‘4Litho”,
166 using fusion inductively coupled plasma emission (FUS-ICP) and inductively coupled
167 plasma emission mass spectrometry (ICP-MS) (for details see
168 http://www.actlabs.com).

169

170 RESULTS

171 *Kaolin petrography*

172 Kaolin samples are made up of soft powder with white to gray, pale yellow and
173 pale brown colors, containing some consolidated fragments.

Particle-size distribution of Caluquembe kaolin shows that silt fraction is predominant whereas clay and sand fractions are less abundant. Therefore, 4.9 to 8.8 vol. % of kaolin particles are less than 2 µm in size; 54.1 to 75.1 vol. % between 2 µm and 63 µm; 12.6 to 17.9 vol. % between 63 µm and 125 µm; and 3.3 to 12 vol. % between 125 µm and 250 µm.

Quartz, microcline, and plagioclase (albite) are set in a finer-grained mass (groundmass) composed by muscovite and kaolinite (Figure 3a). Quartz occurs as irregular fragments of 500 µm in size with typical angular borders. Microcline anhedral grains are up to 200 µm in diameter and they are commonly altered to cryptocrystalline kaolinite. Plagioclase has grain size of less than 100 µm and is also altered to sericite. SEM-BSE images show that in the finer-grained mass, muscovite occurs as tabular habit crystals (50 µm in length) while particles of kaolinite often show a platy habit and are stacked together forming "booklets" or radial aggregates, even both phases can be also found as very fine anhedral particles (Figure 3b). Some particles of muscovite are separated by cleavage (Figure 3c). Kaolinite is also found as muscovite-kaolinite intergrowths (up to 50 µm in length), which could be distinguished using EDS microanalysis (Figure 3b). Phosphate enriched in LREE (Light Rare Earth Elements), probably monazite-(Ce), is also found an accessory mineral phase (Figure 3d).

X-ray powder diffraction (XRPD)

The quantitative analysis of 26 whole-rock random powders (XRPD) show that samples are mainly comprised of kaolinite (50.4 to 87.0 wt. %), quartz (0 to 23.5 wt. %), albite (0.3 to 7.4 wt. %), microcline (1.2 to 21.5 wt. %) and muscovite (1.1 to 29.2

198 wt. %) (Table 1). Scarce hematite (<1 wt. %) is also found in some samples, except in
199 sample KP1, which contains a significant amount of accessory minerals, with 1.6 wt. %
200 of hematite and 2.4 wt. % of calcite. The shallower samples (KA, KU3, KU6B, KKL17B,
201 KL13-2, L-1 and L-2) are richer in kaolinite than samples obtained from base of the
202 profiles. For instance, samples KU6B (shallow) and KU6D (deep) from the same outcrop
203 contain 71.5 wt. % and 58.9 wt. % of kaolinite, respectively (Table 1).

204 XRPD profile refinement for sample KL13-2 reveals a significant percentage of
205 kaolinite (84.2 wt. %), less than 1 wt. % of quartz, and very low muscovite content (2.9
206 wt. %) (Figure 4a). Sample KC12 has higher quartz (23.5 wt. %) and muscovite contents
207 (21.3 wt. %), and less kaolinite (50.4 wt. %). A negative correlation (R^2=0.67) between
208 the wt. % content of kaolinite and muscovite plus K-feldspar is evident in the analyzed
209 samples (Figure 5).

210 The average crystallite size for kaolinite is 15-35 nm, calculated from the profile
211 refinement by XRPD.

212 Five samples containing illite and three samples containing smectite were
213 identified (Table 2). The three smectite-bearing samples (KL6E, KL8E*, and KLB10) are
214 located in the deepest part of the outcrop, containing a low kaolinite grade (Table 2).
215 Illite-bearing samples KK13 and KK11A also contain goethite: 12.9 wt. % and 22.9 wt.
216 %, respectively.

217 The XRPD pattern of three samples show the d_{00l} of illite, muscovite, smectite,
218 and kaolinite in the region of 4° to 15° (2θ) (Figure 6). The d_{002} band for illite at 10.03 Å
219 was broader and less intense than that for muscovite at d_{002}= 9.97 Å. A broad and low
220 intensity maximum for smectite is at d_{001} = 14.9 Å. The d_{001} of kaolinite at 7.14 Å shows

no appreciable differences in the XRPD profile of these samples and is narrow and intense.

In the XRD pattern of oriented mounts samples is possible to distinguish kaolinite, the reflections d_{00l} disappeared after heating to 550 °C. After ethylene glycol treatment there is not variations detected. In contrast, the XRD patterns of oriented mounts of samples with smectite have significant changes. The peak at d_{001} = 14.9 Å changes to 17 Å when solvated in ethylene glycol, and changes to 10 Å when the sample is heated to 550 °C. Samples with illite show only a slight expansion of the broad reflection at d_{002} = 10.03 Å when solvated in ethylene glycol, indicating a small proportion of expanded clay (Thorez, 1975; Moore and Reynolds, 1997).

The physical properties of kaolin, such as whiteness, abrasiveness, particle size, shape and distribution, viscosity, and rheology vary depending on the genetic conditions of the deposits. Kaolinite Crystallinity Index (KCI) may be significant to the calculation of the degree of crystal perfection in kaolinite, which is a necessary parameter to evaluate kaolinite quality for industrial applications, in addition to the plasticity correlation. In the XRPD pattern, reflections 020, $1\bar{1}0$ and $11\bar{1}$ were detected in the region of 20° to 23° (2θ). These reflections are sensitive to random and interlayer displacements and allow calculating for KCI (HI from Hinckley, 1963; IK from Stoch, 1974; AGFI from Aparicio *et al*., 2006). The Hinckley crystallinity index (HI, Hinckley, 1963) is one of the most widely used indices. Normal values range from <0.5 (disordered) to 1.5 (ordered). The calculated HI index in the region of 20° to 23° (2θ) is of 1.06 in sample KA, 1.05 in sample KC12, and 1.09 in sample KL12A. The HI of Caluquembe kaolin is generally higher than reported in other kaolin deposits worldwide such as the sedimentary kaolin from Warren (Georgia, USA) with 0.56 HI or

245 the kaolin from Montecastelo (Spain) presenting 1.00 HI (Aparicio et al. 2006). The IK
246 index or Stoch index (Stoch, 1974) is measured in the same zone as for HI, and the
247 normal values range from >1.0 (disordered) to <0.7 (ordered). The calculated IK index
248 in the region of 20° to 23° (2θ) is 1.04 (disordered) in sample KL12A.

249 According to Aparicio and Galan (1999), the KCI can only be determined as an
250 approximate value. Kaolinite maximums by XRPD are close to the muscovite and
251 quartz maximums in the region of 20° to 23° (2θ) (Figure 4b and 4c). Aparicio *et al*.
252 (2006) present a new AGFI (Aparicio-Galán-Ferrel Index) based on the additional
253 processing to decompose overlapping peaks detected in the region of interest with the
254 software MacDiff (Petschick, 2004).

255 Peak intensities of 020, $1\bar{1}0$ and $11\bar{1}$ in kaolinite has been determined through
256 full profile refinement by XRPD and the software Topas V4.2 in samples from
257 Caluquembe. Sample KC12 has quartz (24 wt. %) and muscovite (21 wt. %), with an
258 AGFI of 1.35 (Figure 4b). Sample KA has <1 wt. % of quartz and 9 wt. % of muscovite,
259 and an AGFI of 1.06 (Figure 4c). Sample KL12A has 5 wt. % of quartz and 20 wt. % of
260 muscovite and an AGFI of 1.19. According to Aparicio *et al*. (2006), these samples can
261 be classified as low and medium defect kaolinite. Similar data were obtained by
262 Aparicio *et al*. (2006) in kaolinite from Mevaiela (Angola). In this case, the AGFI is 1.35
263 in kaolinite containing 20 wt. % of quartz, which suggests that AGFI is more accurate in
264 determining the crystallinity of the sample and is also related to the kaolinite content.

265 *Differential thermal and thermogravimetric analysis (DTA-TGA)*

266 The DTA curve (Figure 7) only shows an endothermic peak in dry air conditions
267 at 540.3 °C in sample KL132, confirming the dehydration of kaolinite (Mackenzie, 1957;
268 Liu *et al*., 2015). Samples have a mass loss between 6.2 and 13.0 wt. % up to 650ºC in

TGA curve. Samples with higher kaolinite contents show a more significant mass loss. The amount of kaolinite calculated by mass loss is between 44.3 and 92.9 wt. % (Table 1).

Correlation between TGA and XRPD

Thermal analyses have been carried out to check the quantitative results of mineral phases calculated by XRPD using the correlation between the calculated wt. % of kaolinite in the profile refinement by XRPD and the calculated wt. % of kaolinite in TGA (Figure 8). Samples containing more kaolinite also have higher mass loss that shows a positive correlation (R^2=0.75). The model proposed demonstrates an adequate accuracy for the quantification of kaolinite and shows that material sampled closer to the surface is richer in kaolinite than samples from the deeper part of the profile. The quantitative results of samples containing illite and smectite give more inaccurate values considering that the thermal characteristics of kaolinite are influenced by the presence of smectite and illite.

Kaolin geochemistry

The average chemical composition of kaolinite determined by EMPA is: 46.28 SiO_2, 36.31 Al_2O_3, 0.58 MgO, 0.03 Na_2O, 0.10 TiO_2, 0.85 Fe_2O_3, 0.03 MnO, 0.04 BaO, 0.07 CaO, 0.05 K_2O wt. %. The average structural formula based on 14 oxygens is the following: $(Al_{3,77}Fe^{3+}_{0,05}Mg_{0,06})_{3.9}\ Si_{4,0}\ O_{10}\ (OH)_{8.}$

Major-, trace- and REE concentrations have been obtained from six representative samples from the Caluquembe area (Table 3 and 4). Two kaolin samples from Uganda (Nyakairu and Koeberl, 2001), one from Cameroon (Njoya *et al*., 2006) and one from Sa Bandeira granite in Huambo (Angola) are also shown for comparison

292 in Tables 3 and 4. Sa Bandeira granite has a very similar composition to the granites
293 that outcrop in the Caluquembe area (Montenegro de Andrade, 1954).

294 Major elements generally show a different trend in the altered sample
295 compared to the parent rock (Table 3). The SiO_2 trend of Caluquembe kaolin is
296 decreasing and the Al_2O_3 trend is increasing compared to the granite from Sa Bandeira.
297 SiO_2 is high for all samples ranging between 45.35 and 63.24 wt. %. Al_2O_3 contents lie
298 between 21.89 and 32.24 wt. %. Fe_2O_3 is between 1.36 and 4.25 wt. %. K_2O is between
299 1.16 and 4.03 wt. %. TiO_2 is between 0.49 and 0.86 wt. %. Other remaining oxides (Mn,
300 Mg, Ca, Na) are only present as traces (<0.2 wt. %). Loss on ignition (LOI) values are
301 between 7.80 and 13.69 wt. %.

302 The most abundant trace elements are: Zr from 162 (sample L1) to 430 (sample
303 K6E) ppm; Ba from 222 (sample K6E) to 1090 (sample KL13-2) ppm; Rb from 54
304 (sample KL13-2) to 206 (sample KLB 10) ppm. Other trace elements such as Sc, V, Cr,
305 Co, Ni, Cu, Zn, Ga, Sr, Y, Nb, Hf, Pb, Th, and U are usually less than 100 ppm. As, Mb,
306 Ag, In, Sn, Sb, Cs, Ta, W and Bi are less than 5 ppm (Table 4).

307 REE contents in kaolin samples vary from 130 ppm (sample L1) to 564 ppm
308 (sample KL13-2). REY (REE+Y) range between 142 ppm and 624 ppm. LREE (Light Rare
309 Earth Elements) (La, Ce, Pr, Nd, Sm, Eu) range from 524 to 122 ppm while HREE (Heavy
310 Rare Earth Elements) (Gd, Tb, Dy, Ho, Er, Tm, Yb, Lu) range from 40 to 8 ppm (Table 4).
311 The C1 chondrite-normalized REE plots (Figure 9a) (McDonough and Sun, 1995) are
312 roughly parallel and characterized by negative slopes as a result of enrichment in the
313 LREE relative to HREE. The normalization via upper Continental Crust (UCC, Rudnick
314 and Gao, 2003) is presented in Figure 9b. In general, Caluquembe samples present flat

315 REE patterns with high values of HREE, which is a relative significant enrichment similar
316 to that reported in kaolin from Warren (Georgia, USA) from heavy, light and grit
317 fractions (Elliott *et al*. 2018). They also have a negative Sc anomaly as reported in
318 heavy and grit mineral fractions from Warren kaolin too. Only sample L-1 from
319 Caluquembe has a different behaviour with and Sc enrichment as light fraction from
320 Jeffersonville Member and Buffalo Creek in Georgia, USA.

321 DISCUSSION

322 *Classification of the Caluquembe deposit*

323 Considering the little available geological information about this area, it is
324 necessary to establish a formal classification of the Caluquembe kaolin deposit using
325 the mineralogical and compositional data obtained in the present work.

326 Kaolinite from Caluquembe is generally found as finer-grained mass of particles,
327 though also reported as muscovite-kaolinite intergrowths. Considering the results of
328 the granulometric curve, particle size distribution of the Caluquembe kaolin shows
329 small amounts of the fraction below 4 μm (8.7 to 13.8 vol. %), which correspond to the
330 kaolinite that originated by alteration of potassium feldspars, while muscovite-
331 kaolinite intergrowths may correspond to the fraction below 63 μm (74.0 to 83.9 vol.
332 %).

333 The Chemical Index of Alteration (CIA) is also a very suitable parameter to
334 determine the weathering level of feldspars and the corresponding formation of kaolin
335 by this process (Nesbitt and Young, 1984). CIA is expressed from 0 to 100 and it is
336 calculated using the main compositional elements of kaolin: Al, Na, K, and Ca
337 [$CIA=Al_2O_3 /(Al_2O_3+Na_2O+K_2O+CaO)\cdot 100$]. The CIA parameters of the Caluquembe

kaolin have indexes from 82 to 95 (Table 3), which are significantly high and indicate an elevated level of feldspar alteration. In addition, it is possible to distinguish changes in the CIA parameter comparing kaolin samples obtained in the same outcrop from different depths in the profile. For instance, in sample KU6B (upper level) and sample KU6D (lower level), the CIA parameter is 87 and 82 respectively, indicating a significant increase of weathering in the upper levels which is also directly related to the kaolinite content: 71.5 and 58.9 wt. %, respectively.

During intense weathering, potassium feldspar and plagioclase are destabilized and transformed to kaolinite, while sericite and muscovite are also transformed to kaolinite especially in the upper levels of the profile (Galan, 2006). This would explain why kaolinite content decreases towards the deeper parts of the weathering profile as reported in the samples from the Caluquembe area.

The concentration ratio of La/Th as well as Y/HREE may also be useful parameters to determine kaolin provenance. In the case of Caluquembe kaolin, La/Th ratio is 2.7, which is similar to values reported in upper continental crust (2.8 ±0.2), indicating a felsic source for kaolin (Taylor and McLeman, 1995). On the other hand, Y/HREE ranges from 1.2 and 1.5, indicating a similar process during kaolinization.

Eu anomalies associated to more evolved continental crust are found, for instance, in clay-rich sediments from central Uganda (Nyakairu and Koeberl, 2001), in samples from weathered granitic rocks of south China (Bao and Zhao, 2008), in samples from Sögüt from northwetern Turkey (Kadir and Kart, 2009) and in samples from residual kaolin derived from granitic rock in SE Germany (Dill, 2016). This Eu anomaly is not found in samples from Caluquembe (Figure 9, Table 4).

We consider that all these compositional and mineralogical features of the kaolin deposits from the Caluquembe area should be regarded as strong evidence indicating that they originated from the weathering of precursor granitic rocks. Therefore, kaolin deposits from Caluquembe should be classified as primary type kaolin deposits (Dill, 2016).

Economic interest

The potential extension of kaolin outcrops in Caluquembe is estimated around 20 km^2, achieving a significant thickness that ranges from 5 to 10 meters (Figure 2). At present, a further evaluation is being carried out in the area to obtain a more accurate calculation of the extension and thickness of the kaolin deposits. However, the preliminary estimation concludes that potential inferred reserves of kaolin in the Caluquembe area are estimated around 500,000,000 m^3. Although this calculation is approximate and more accurate studies are necessary, this preliminary volume would suggest that Caluquembe is a medium-size kaolin deposit, bigger than other deposits from Western Africa such as Makoro, Botswana (Ekosse, 2000).

Al_2O_3 contents of kaolin are directly related to the kaolinite percentage and are consequently considered as a significant parameter to determine kaolin quality. Caluquembe Al_2O_3 contents (21.9 to 32.2 wt. %) and SiO_2/Al_2O_3 ratio (1.28) are similar to those reported for kaolin from the Zhanjiang, Longyan and Dazhou deposits (Guangdong Province, China; Wilson *et al*., 1997), and slightly higher than the theoretical value for kaolinite (1.16). However, Fe_2O_3 contents of Caluquembe kaolin are quite significant (1.4 to 4.3 wt. %) and they should be considered as penalizing for

384 the potential marketing of the Caluquembe kaolin (Saikia *et al*., 2003, Lopez Galindo *et*
385 *al*., 2007).

386 The mineralogical and chemical compositions of kaolin from Caluquembe are
387 similar to other African kaolins. In addition, the kaolinite grade is slightly lower or
388 similar to those found in Koutaba and Mayouom in Cameroon (Nkalih Mefire *et al*.,
389 2015; Njoya *et al*., 2006), central Uganda (Nyakairu *et al*., 2001), Makoro in Botswana
390 (Ekosse, 2000) and Grahamstown in South Africa (Heckroodt, 1991) (Table 5). The
391 mineralogical composition of three classical kaolin deposits developed from precursor
392 granites is presented for comparison in the Table 5: Guandong (China), Otovice (Czech
393 Republic) and Cornwall (England.) All of them have higher kaolinite contents than the
394 Caluquembe deposit.

395 Considering the main features of Caluquembe kaolin, the suitable application of
396 this material should be focused on the fabrication of bricks, pavers, roofing tiles and
397 the ceramics industry (Heckroodt, 1991; Gomes *et al*., 1994; Savianno *et al*., 2005;
398 Ekosse, 2000; Nyakairu *et al*., 2001; Njoya *et al*., 2006; Ekosse, 2010 ; Nkalih Mefire *et*
399 *al*., 2015).

400 In addition, kaolin deposits have recently been considered non-conventional
401 sources of critical metals such as REE (Aagaard, 1974; Laufer et al., 1984; Xiao et al.,
402 2016; Sanematsu and Watanabe, 2016; Elliot et al., 2018). Values of ∑REE (La, Ce, Pr,
403 Nd, Sm, Eu, Gd, Tb, Dy, Ho, Er, Tm, Yb, Lu) in Caluquembe are highly erratic 129.58
404 ppm to 563.5 ppm, Table 4 and do not show a correlation with SiO_2, Fe_2O_3, CaO, P_2O_5
405 and MnO. Samples are more enriched in LREE (Table 4) and the ratio LREE/HREE is
406 homogeneous by a mean factor ~ 14. A good positive correlation exists between Y and
407 REE (R^2=0.98) and between Y and HREE (R^2=0.99). The correlation between REY and

kaolinite wt. % is positive (R^2=0.75) except in sample L-1. A positive correlation is shown between Y and kaolinite wt. % (R^2=0.78) for except sample L-1. In some samples from the Caluquembe area, the REY content is higher than 600 ppm (Table 4), which is higher than that reported in other deposits, for instance, in Uganda and Cameroon (Table 4). Therefore, considering the medium size of the Caluquembe kaolin deposit (Sanematsu and Watanabe, 2016) this can be considered as a potential non-conventional source of REY. However, more detailed studies will be necessary to determine which mineral phases are enriched in REE and their relationship between the kaolinite contents and the corresponding potential extraction of REY as a subproduct during kaolinite exploitation.

CONCLUSIONS

The present work is the first study of the recently discovered kaolin deposit from the Caluquembe area (Angola).

The studied kaolin samples do not have significant compositional and mineralogical differences. Kaolinite contents calculated from full profile refinement by XRPD range between 50.4 and 87.0 wt. % and between 44.3 and 92.9 wt. %, calculated with TGA (Figure 8). The samples that outcrop in shallower areas are richer in kaolinite than deeper samples. A relevant conclusion of the present work is that full profile fitting by XRPD and TGA results have a good correlation, and the combination of both techniques is suitable to determine kaolinite contents in this type of clay deposits.

Mineralogy and compositional features of kaolin samples indicate that Caluquembe deposits were generated by weathering of granitic rocks and the

corresponding alteration of feldspars. Therefore, they should be classified as primary kaolin deposits.

The economic importance of these deposits is considered to be very relevant, especially considering that they are located in an underdeveloped region. The mineralogical and compositional features of the Caluquembe kaolin and its low to medium crystallinity indicate that the most suitable application for this clay is the manufacture of structural products, such as bricks, pavers and roofing tiles. Caluquembe kaolin would need to be refined and processed to be used in other applications, such as in the pharmaceutical industry or in the production of paper and cosmetics.

The chondrite-normalized rare earth element (REE) patterns show enrichment in the light REEs, absence of an Eu anomaly and a positive correlation has been found between kaolinite wt. % and REY content. Upcoming studies will be necessary to characterize REY contents and REY carrier mineral phases, however, their evaluation as a sub product in a possible future kaolinite exploitation is highly recommended.

Due to the high content of kaolinite in the deposit of Caluquembe, this area is very suitable for the exploration and potential exploitation of kaolinite, a very valuable raw material with a bright future.

ACKNOWLEDGMENTS

This research was supported by the CGL2012-36263, CGL2006-12973 and CGL2009-13758 projects of the *Ministerio de Ciencia e Innovación* of the Spanish Government, the AGAUR 2014SGR01661 project of the *Generalitat de Catalunya* and

by a FI grant to J. Xu (coded FI_B 00904) sponsored by the *Secretaria d'Universitats i Recerca* of the *Departament d'Economia i Coneixement* of the *Generalitat de Catalunya*. The authors thank the Scientific and Technical Centers of the University of Barcelona (CCiTUB) for their support in carrying out experimental analyses.

REFERENCES

Aagaard, P. (1974) Rare earth elements adsorption on clay minerals. *Bulletin du groupe français des argiles*, **26**, 193-199.

Aparicio, P. and Galan, E. (1999) Mineralogical interference on kaolinite crystallinity index measurements. *Clays and Clay Minerals*, **47**, 12-27.

Aparicio, P., Galan, E. and Ferrell, R.E. (2006) A new kaolinite order index based on XRD profile fitting. *Clay Minerals*, **41**, 811–817.

Ashwal, L.D., Twist, D. (1994) The Kunene complex, Angola/Namibia: a composite massif-type anorthosite complex. *Geological Magazine*, **131**, 579-591.

Bailey, S.W. (1980) Structure of layer silicates. Pp. 1-123 in: *Crystal structure of Clay Minerals and their X-ray Identification* (G.W. Brindley and G. Brown, editors). Monograph, **5**. Mineralogical Society, London.

Bao, Z. and Zhao, Z. (2008) Geochemistry of mineralization with exchangeable REY in the weathering crusts of granitic rocks in South China. *Ore Geology Reviews*, **13,** 519-535.

Bish, D.L. (1993) Rietveld refinement of the kaolinite structure at 1.5 K. *Clays and Clay Minerals*, **41**, 738-744.

Bermúdez-Lugo, O. (2014) Angola and Namibia, Minerals years book. U.S. Geological Survey.

De Carvalho, H., Tassinari, C., Alves, P., Guimaraes, F., Simoes, M.C. (2000) Geochronological review of the Precambrian in western Angola: Lings with Brazil. *Journal of African Earth Sciences*, **31**, 383-402.

Detellier, C. and Schoonheydt, R.A. (2014) From Platy Kaolinite to Nanorolls. *Elements*, **10**, 201-206.

Dedzo, G.K. and Detellier, C. (2016) Functional nanohybrid materials derived from kaolinite. *Applied Clay Science*, **130**, 33-39.

Dill, H. G. (2016) Kaolin: Soil, rock and ore. From the mineral to the magmatic, sedimentary and metamorphic environments*. Earth-Science Reviews*, **161**, 16-129.

Ekosse, G-I (2000) The Makoro kaolin deposit, southeastern Botswana: its genesis and possible industrial applications. *Applied clay science*, **16**, 301-320.

Ekosse, G-I. (2010) Kaolin deposits and occurrences in Africa: Geology, mineralogy and utilization. *Applied Clay Science*, **50**, 212-236.

Elliot. W.C., Gardner, D.J., Malla, P., Riley, E. (2018) A New Look at the Occurrences of the Rare-Earth Elements in the Georgia Kaolins. *Clays and Clay Minerals*, **66** (3), 245-260.

Flanagan, M.D. (2016) *Clays in Mineral Commodity summaries*. U.S. Geological Survey, **50**.

Galán, E. (2006) Genesis of clay minerals Pp 1129-1162 in Handbook of clay science. (Bergaya, F.; Theng, B.K.G. and Lagaly, G. editors) Developments in clay science 1. Elsevier.

Galán, E., Aparicio, P., Fernández-Caliani, J.C., Miras, A., G.Márquez, M, Fallick, A. and Clauer, N. (2016) New insights on mineralogy and genesis of kaolin deposits:The Burela kaolin deposit (Northwestern Spain). *Applied Clay Science*, **131**, 14-26.

501 Gomes, C., Velho, J.A. and Guimaraes F. (1994) Kaolin deposit of Mevaiela (Angola)
502 alteration product of anorthosite: assessment of kaolin potentialities for
503 applications in paper. *Applied Clay Science*, **9**, 97-106.
504 Guggenheim, S., Adams, J.M., Bain, D.C., Bergaya, F., Brigatti, M.F., Drits, V.A.,
505 Formoso, M.L.L., Galán, E., Kogure, T. and Stanjek, H. (2006) Summary of
506 recommendations of nomenclature committees relevant to clay mineralogy: report
507 of the Association Internationale pour l'etude des Argiles, nomenclature committee
508 for 2006. *Clay Minerals*, **41**, 863-877.
509 Hanson, R.E. (2003) Proterozoic geochronology and tectonic evolution of southern
510 Africa. *In:* Yoshida, M., Windley, B.F, Dasgupta, S (eds). Proterozoic East Gondwana:
511 Supercontinent Assembly and Breakup. Geological Society of London, Special
512 Publications, **206**, 427-463.
513 Heckroodt, R.O. (1991) Clay and clay materials in South Africa. *Journal of the south*
514 *African institute of mining and metallurgy,* **91**, 343-363.
515 Hinckley, D.N. (1963) Variability in "crystallinity" values among the kaolin deposits of
516 the coastal plain of Georgia and South Carolina. *Clays and Clay Minerals*, **11**, 229-
517 235.
518 Jelsma, H., Perrit, S.H., Armstrong, R.A., Ferreira, H.F. (2011) SHRIMP U-Pb zircon
519 geochronology of basement rocks of the Angolan Shield, western Angola. In:
520 *Proceedings of the 23rd CAG, Johannesburg.* Council for Geoscience, Pretoria 203.
521 Kadir, S. and Kart, F. (2009) The occurrence and origin of the Sögüt kaolinite deposits in
522 the Paleozoic Saricayaka granite-granodiorite complexes and overlying Neogene
523 sediments (Bilecik, northwestern Turkey). *Clays and clay Minerals*, **57**, 311-329.

524 Laufer, F., Yariv, S. and Steinberg, M. (1984) The adsorption of quadrivalent cerium by
525 kaolinite. *Clay Minerals*, **19**, 137-149.
526 Liu, X., Liu*, X. and Hu, Y. (2015) Investigation of the thermal behaviour and
527 decomposition kinetics of kaolinite. *Clay Minerals*, **50**, 199–209
528 López-Galindo, A., Viseras, C. and Cerezo, P. (2007) compositional, technical and safety
529 specifications of clays to be used as pharmaceutical and cosmetic products. *Applied*
530 *Clay Science*, **36**, 51-63.
531 MacKenzie, R.C. (1957) *The Differential Thermal Investigation of Clays*. Mineralogical
532 Society (Clay Minerals Group), London, 456 pp.
533 Mansa, R., Ngassa Piegang, G. B. and Detellier, C. (2017) Kaolinite aggregation in book-
534 like structures from non-aqueous media. *Clays and Clay Minerals,* **65**, 193–205.
535 Marques, M. M. (1977) Esboço das grandes unidades geomorfológicas de Angola (2ª
536 aproximação). Instituto de Investigaçao Cientifica Tropical, Garcia de Orta, Sérvicio
537 Geologico, Lisboa, **2(1)**, 41-43.
538 Mayer, A., Hofmann, A.W., Sinigoi, S., Morais, E. (2004) Mesoproterozoic Sm-Nd and
539 U-Pb ages for the Kunene Anorthosite Complex of SW Angola. *Precambrian*
540 *Research*, **133**, 187-206.
541 McCourt, S., Armstrong, R.A., Jelsma, H., Mapeo, R.B.M. (2013) New U-Pb SHRIMP ages
542 from the Lubango region, SW Angola: insights into the Palaeoproterozoic evolution
543 of the Angolan Shield, southern Congo Craton, Africa. *Journal of the Geological*
544 *Society of London*, **170**, 353-363.
545 McDonough, W.F. and Sun, S.S. (1995) The composition of the earth. *Chemical*
546 *Geology*, **120**, 223-225.

547 Montenegro de Andrade, M. (1954) *Rochas graníticas de Angola*. Memórias, série
548 geológica IV. Ministério do Ultramar, 464 pp.
549 Moore, D.M. and Reynolds, R.C.Jr. (1997) *X-Ray Diffraction and the Identification and*
550 *Analysis of Clay Minerals*. Oxford University Press, 332 pp.
551 Murray, H.H. (1999c) Applied clay mineralogy today and tomorrow. *Clay Minerals*, **34**,
552 39-49.
553 Murray, H.H. (2000) Traditional and new applications for kaolin, smectite, palygorskite:
554 a general overview. *Applied Caly Science*, **17**, 207-221.
555 Nesbitt, H.W. and Young, G.M. (1984) Prediction of some weathering trends of
556 plutonic and volcanic rocks based on thermodynamic and kinetic considerations.
557 *Geochimica and Cosmochimica Acta*, **48**, 1523-1534.
558 Nkalih Mefire, A., Njoya, A., Yongue Fouateu, R., Mache, J. R., Tapon, N.A., Nzeukou
559 Nzeugang, A., Melo Chinje, U., Pilate, P., Flament, P., Siniapkine, S., Ngono, A. and
560 Fagel, N. (2015) Occurrences of kaolin in Koutaba (west Cameroon): Mineralogical
561 and physicochemical characterization for use in ceramic products. *Clay Minerals*, **50**,
562 593–606.
563 Nguie, G., Dedzo, G.K. and Detellier, C. (2016) Synthesis and catalytic application of
564 palladium nanoparticles supported on kaolinite-based nanohybrid materials. *Dalton*
565 *Transactions*, 45.
566 Njoya, A., Nkoumbou, C., Grosbois, C., Njopwouo, D., Njoya, D., Courtin-Nomade, A.,
567 Yvon, J. and Martin, F. (2006) Genesis of Mayouom kaolin deposit (western
568 Cameroon). *Applied Clay Science*, **32**, 125-140.

569 Nyakairu, G. W. A. and Koeberl, C. (2001) Mineralogical and chemical composition and
570 distribution of rare earth elements in clay-rich sediments from central Uganda.
571 *Geochemical Journal*, **35**, 13-28.
572 Nyakairu, G. W. A., Koeberl, C. and Kurzweil, H. (2001) The Buwambo kaolin deposit in
573 central Uganda: Mineralogical and chemical composition. NOTE, *Geochemical*
574 *Journal*, **35**, 245-256.
575 Petschick, R. (2004) *MacDiff* 4.2.5. http://servermac.geologie.uni-
576 frankfurt.de/Rainer.html.
577 Phipps, J.S. (2014) Engineering minerals for performance applications: an industrial
578 perspective .*Clay Minerals*, **49**, 1–16
579 Pruett, R.J. (2016) Kaolin deposits and their uses: Northern Brazil and Georgia, USA.
580 *Applied Clay Science*, **131**, 3-13.
581 Rudnick, R.L. and Gao, R. (2003) Composition of the continental crust. Pp. 1-64 in: The
582 Crust (R.L. Rudnick, editor). Treatise of Geochemistry, 3. Elsevier-Pergamon, Oxford,
583 UK.
584 Saikia, N., Bharali, D., Sengupta, P., Bordolo, D., Goswamee, R., Saikia, P. and Borthakur
585 P.C. (2003) Characterization, beneficiation and utilization of a kaolinite clay from
586 Assam, India. *Applied Clay Science*, **24**, 93-103.
587 Sanematsu, K. and Watanabe, Y. (2016) Characteristics and Genesis of Ion Adsorptio-
588 Type Rare Earth Element Deposits. *Reviews in Economic Geology*, **18**, 55-79.
589 Savianno, G., Violo, M., Pieruccini, U., lopes da Silva, E.T. (2005) Kaolin deposits from
590 the northern sector of the Cunene Anorthosite Complex (southern Angola). *Clays*
591 *and Clay Minerals*, **53**, 674-685.

592 Schroeder, P.A. and Erickson, G. (2014) Kaolin: From Ancient Porcelains to
593 Nanocomposites. *Elements*, **10**, 177–182.
594 Silva M.V.S., 1973b. Carta Geologica de Angola. Folha N 207 Gungo. Scale 1:100 000.
595 Silva, A.T.S.F. and Simões, M.V.C. (1980/1981) Geologia da região de Caluquembe
596 (Angola), *Livro de Homenagem ao Professor Doutor Carlos Teixeira pela sua*
597 *jubilação, Bol. Soc. Geol. Portugal*, **22**, 363-375.
598 Stoch L. (1974) *Mineraly Ilaste ('Clay Minerals')*. Geological Publishers, Warsaw, 186-
599 193.
600 Taylor, S.R. and McLennan, S.H. (1995) The geochemical evolution of the continental
601 crust. *Reviews of Geophysics*, **33**, 241-265.
602 TOPAS (2009) *General Profile and Structure Analysis Software for Powder Diffraction*
603 *Data,* version 4.2, Bruker AXS Gmbh, Karlsruhe, Germany, 2009.
604 Thorez, J. (1975) *Phyllosilicates and clay minerals. A laboratory handbook for their X-*
605 *ray diffraction analysis*. Lelotte (Disno), France, 580 pp.
606 Wilson J.R., Halls, C. and Spiro, B. (1997) A comparison between the China clay
607 deposits of China and Corwall. Proceedings of the Usher Society, **9**, 195-200.
608 Xiao, Y., Huang, L., Long, Z.,Feng, Z. and Wang, L. (2016) Adsorption ability of rare earth
609 elements on clay minerals and its practical performance. *Journal of rare earths*, **34,**
610 5, 543-548.
611 Young, R.A. and Hewat, A.W. (1988) Verification of the triclinic crystal structure of
612 kaolinite. *Clays and Clay Minerals*, **36**, 225-232.
613
614

615 ## FIGURE CAPTIONS

616 **Figure 1.** (a) Simplified geological map of Angola (Silva, 1973b); (b) Geological map the
617 Caluquembe region and location of the studied samples.

618 **Figure 2.** Views of kaolin outcrops from the Caluquembe area: (a) Plain areas with
619 typical surface alteration due to significant iron contents; (b), (c) and (d) kaolinite
620 outcrops in rivers and creeks of the Caluquembe area.

621 **Figure 3.** Backscattered electron images (SEM-BSE) of sample Q-2: (a) quartz (Qtz) and
622 feldspars (Fsp) settled in a finer-grained mass consisting of kaolinite (Kln) and
623 muscovite; (b) Intergrowths of kaolinite (Kln) and muscovite (Ms) scattered in a
624 groundmass comprised of kaolinite; (c) Muscovite (Ms) layers separated along
625 cleavage surfaces; (d) REE phosphate and K-feldspars (Fsp) in a groundmass made up
626 of kaolinite (Kln) forming booklets that are often radial.

627 **Figure 4.** (a) XRPD profile refinement (by Topas V4.2 software) of sample KL13-2. The
628 red line corresponds to the calculated profile while the blue line corresponds to the
629 experimental profile. The Bragg positions of mineral phases are shown at the bottom,
630 Rwp= 8.7 (agreement with weighted profile factor in the Rietveld method); (b) XRPD
631 profile refinement of sample KC12 in the region 17º-30º 2Θ. The blue thick line
632 corresponds to the experimental XRD profile of this sample. The green line
633 corresponds to the calculated XRD profile of kaolinite and d-spacing for 020 reflection
634 for kaolinite is 4.4719Å, for $1\bar{1}0$ is 4.3649Å and for $11\bar{1}$ is 4.1803Å. The blue and purple
635 lines correspond to calculated XRD profiles of quartz and muscovite, respectively, also
636 included the calculated XRD profiles of hematite, albite low and microcline, Rwp=14.1;

637 (c) XRPD profile refinement of sample KA in the region 17º-30º 2Θ. The blue thick line
638 corresponds to the experimental XRD profile of this sample. The green line
639 corresponds to calculated XRD profile of kaolinite. The d-spacing for 020 reflection of
640 kaolinite is 4.4694Å, for $1\bar{1}0$ is 4.3628Å and for $11\bar{1}$ is 4.1795Å. The blue and purple
641 lines correspond to calculated XRD profile of quartz and muscovite, respectively, also
642 included the calculated XRD profiles of hematite, albite low and microcline, Rwp=11.3.

643 **Figure 5.** Relation between muscovite+K-feldspar vs. kaolinite (wt. %) calculated by
644 XRPD profile refinement with Topas V4.2.

645 **Figure 6.** XRPD of samples in the region from 4° to 15° 2Θ: (a) KL13-2, muscovite and
646 kaolinite; (b) KL6E muscovite, kaolinite, and smectite; (c) KK8, muscovite, kaolinite, and
647 illite.

648 **Figure 7.** DTA-TGA curves of kaolin from Calumquembe of sample KL13-2. DTA (black
649 line) - TGA (gray line).

650 **Figure 8.** Kaolinite content (wt. %) calculated by XRPD with Topas V4.2 vs. kaolinite
651 content (wt. %) calculated by mass loss in TGA.

652 **Figure 9.** The enrichment/depletions of REE of Caluquembe kaolin samples: a) Results
653 normalized to C1 chondrite (McDonough and Sun, 1995); b) Results normalized to UCC
654 (Rudnick and Gao, 2003).

655 **TABLES**

656 **Table 1.** Mineral content (wt. %) calculated by XRPD profile refinement with Topas
657 V4.2. Temperature of dehydration (Tm) of kaolinite, mass loss and kaolinite content
658 (wt. %) calculated by TGA.

659 **Table 2.** Mineral content (wt. %) calculated by XRPD profile refinement with Topas
660 V4.2 in samples with smectite and illite. Temperature of dehydration (Tm) of kaolinite,
661 mass loss and kaolinite content (wt. %) calculated by TGA.

662 **Table 3.** Major elements composition of kaolin samples (wt.%) from Caluquembe,
663 Angola; sample BW-1 from Buwambo, and MG-1 from Migade, Uganda (Nyakairu *et*
664 *al*., 2001); sample MY03 from Mayouom, Cameroon (Njoya *et al*., 2006); granite from
665 Sa Bandeira, Angola (Montenegro de Andrade, 1954).

666 **Table 4.** Trace and REE elements (ppm) of samples from Caluquembe, Angola; sample
667 BW-1 from Buwambo, and MG-1 from Migade, Uganda (Nyakairu et al., 2001); sample
668 MY03 from Mayouom, Cameroon (Njoya et al., 2006). n.d =not detected, <dl= <to
669 detection limits

670 **Table 5.** Mineralogical composition determined by XRPD (wt.%) of different kaolin
671 deposits from Africa (Angola, Cameroon, Uganda, South Africa, Botswana) and
672 worldwide (China, Czech Republic and England).

673

Figure 1

Click here to access/download;Figure;Fig_1.jpg

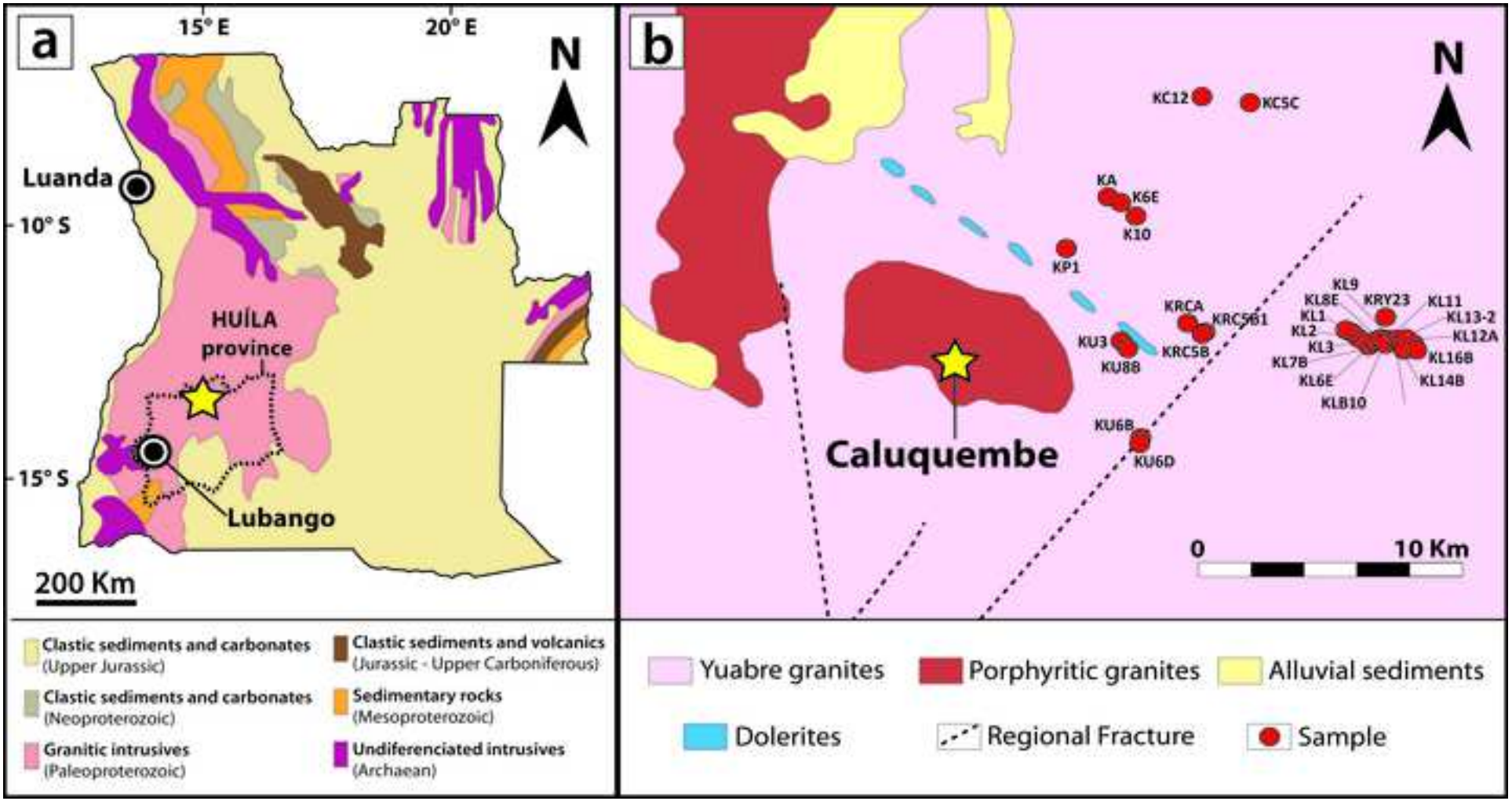

Figure 2

Click here to access/download;Figure;Fig_2.jpg

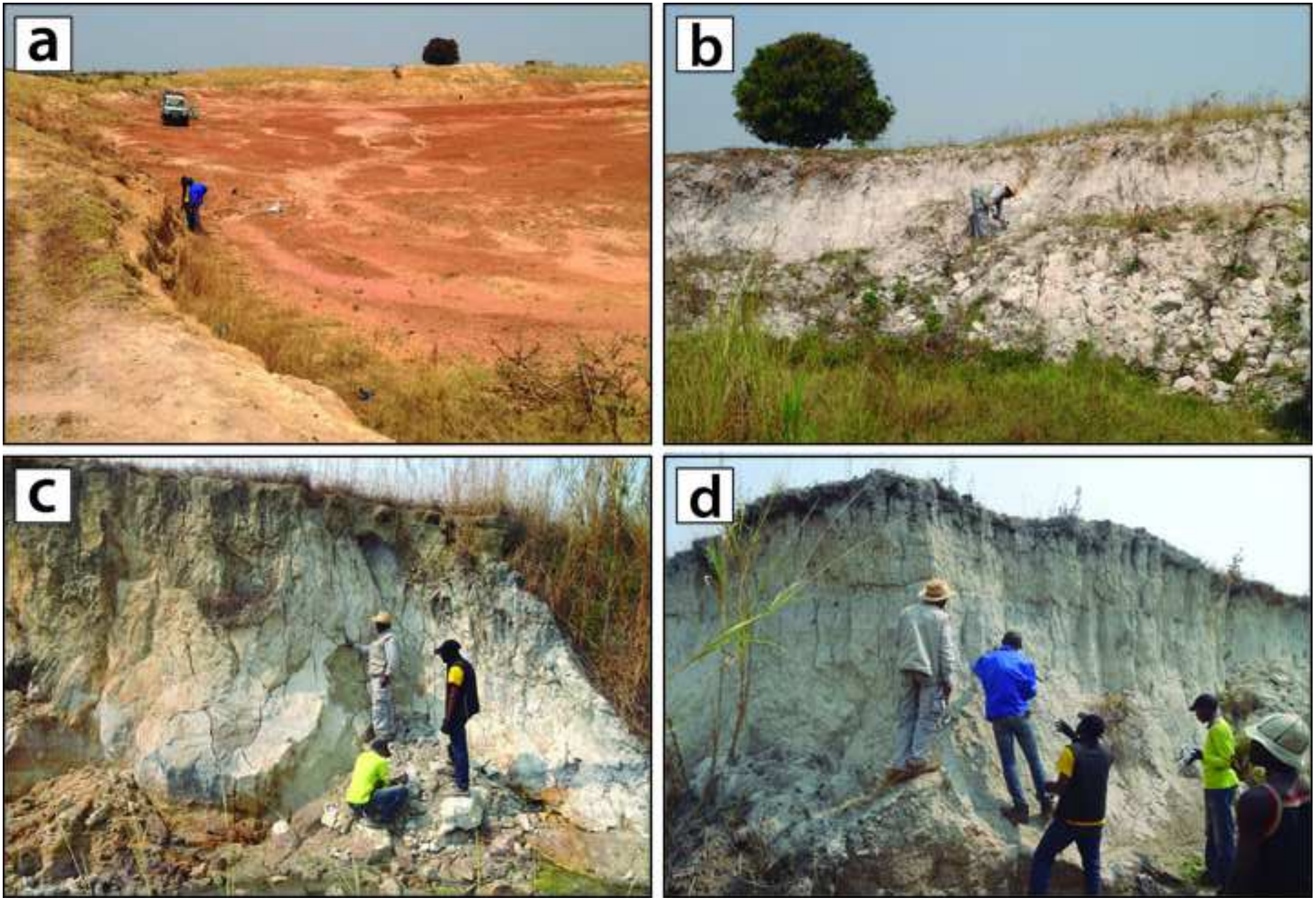

Figure 3

Click here to access/download;Figure;Fig_3.jpg

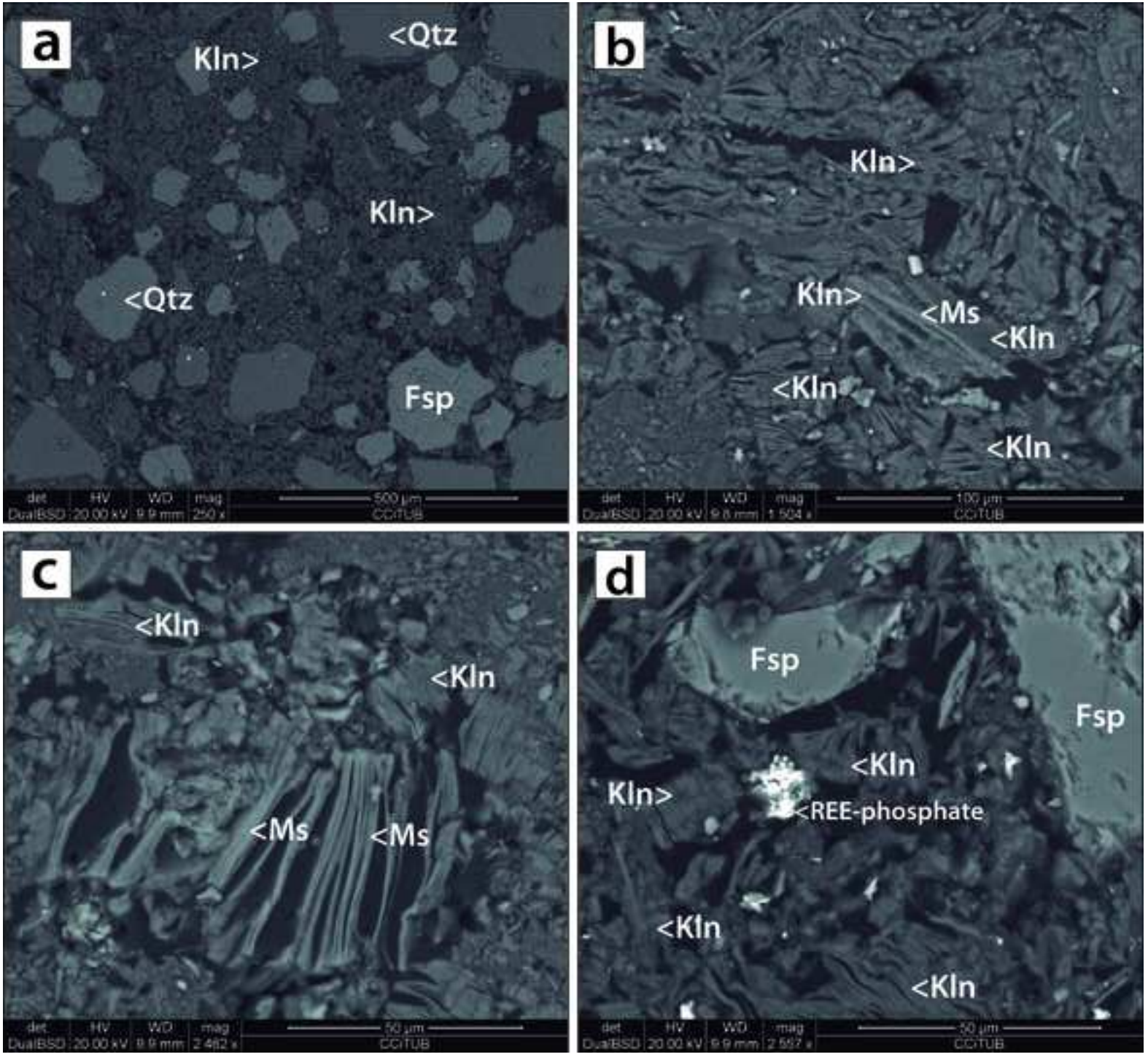

Figure 4

Click here to access/download;Figure;Fig_4.jpg

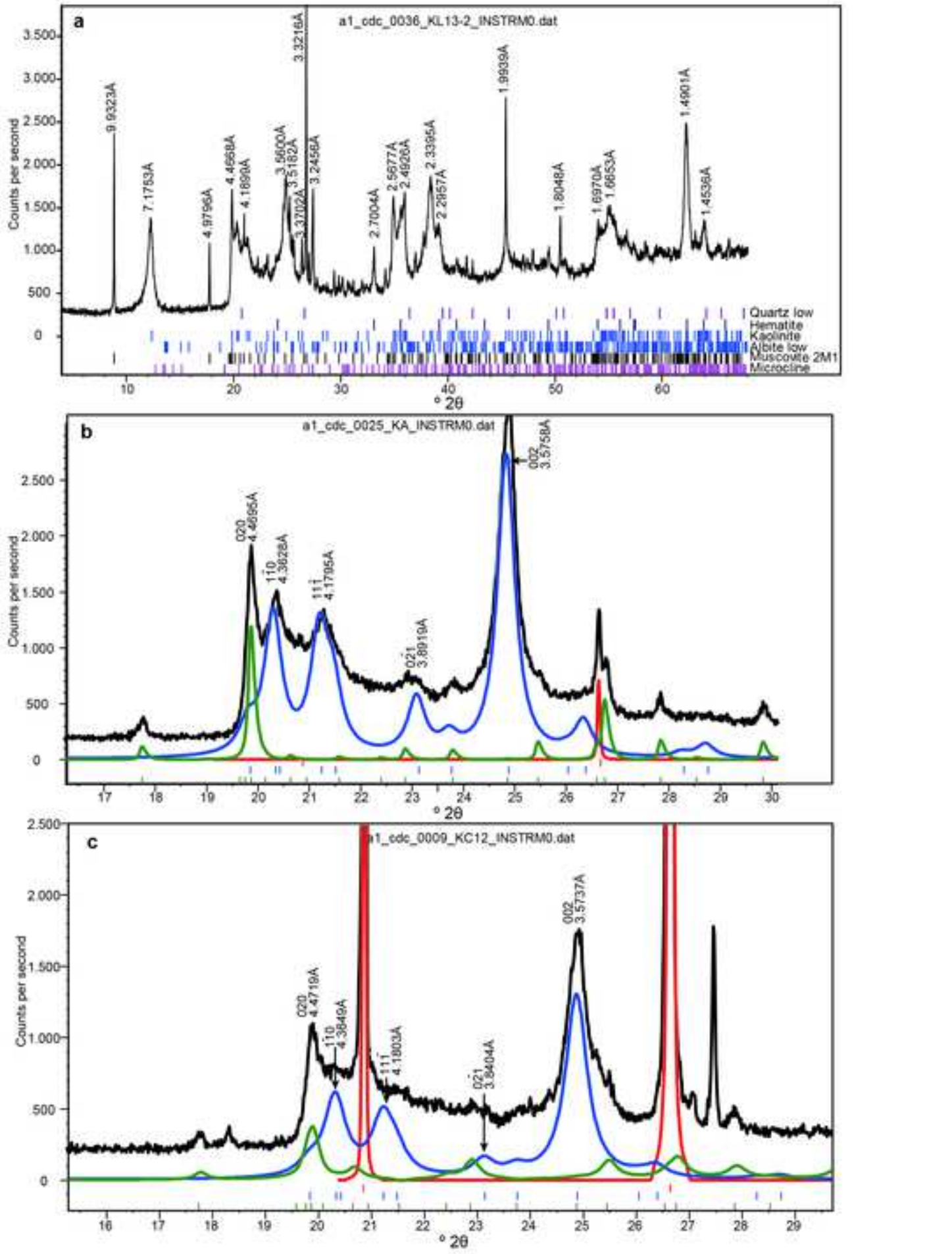

Figure 5

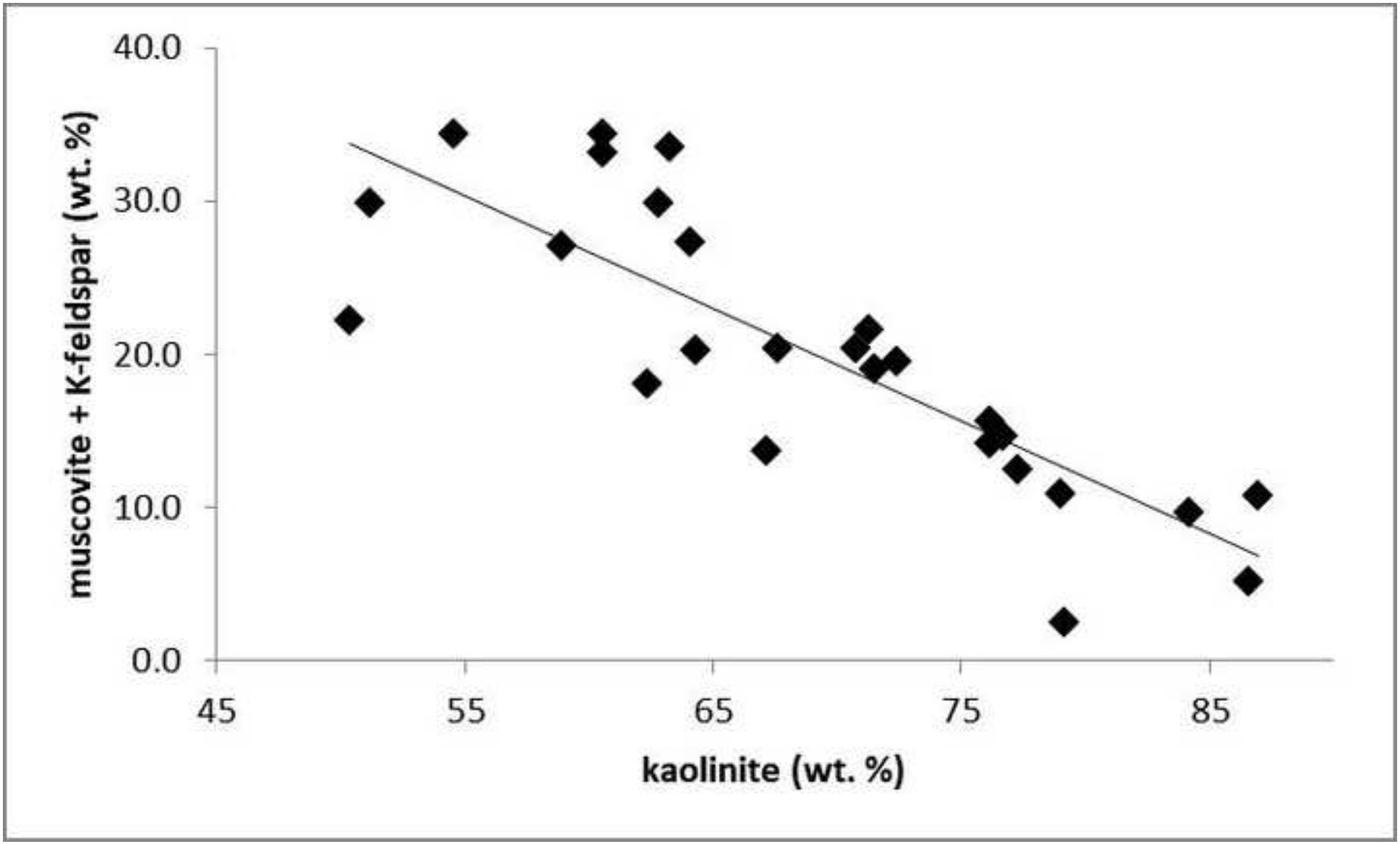

Figure 6

Click here to access/download;Figure;Fig_6.jpg

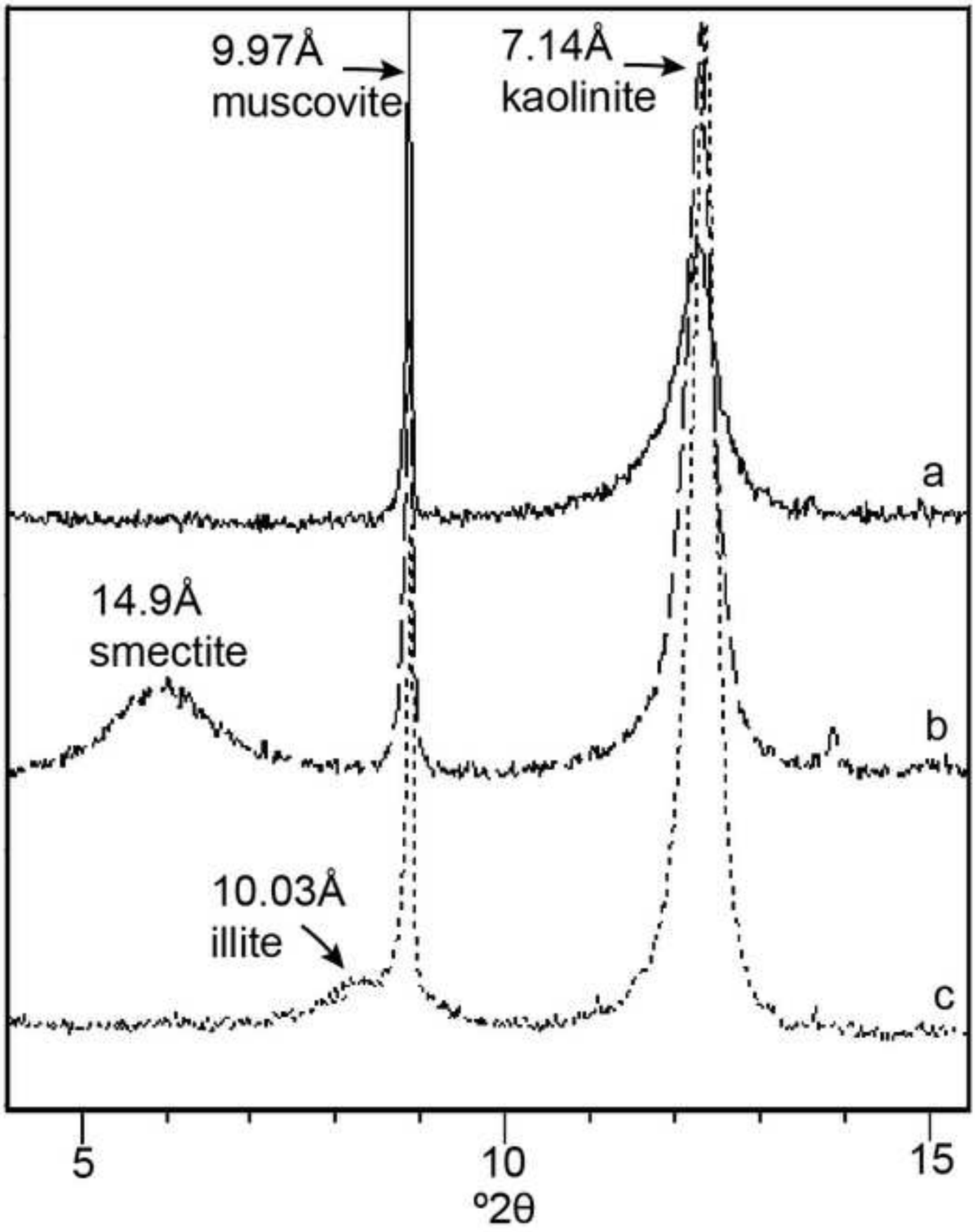

Figure 7

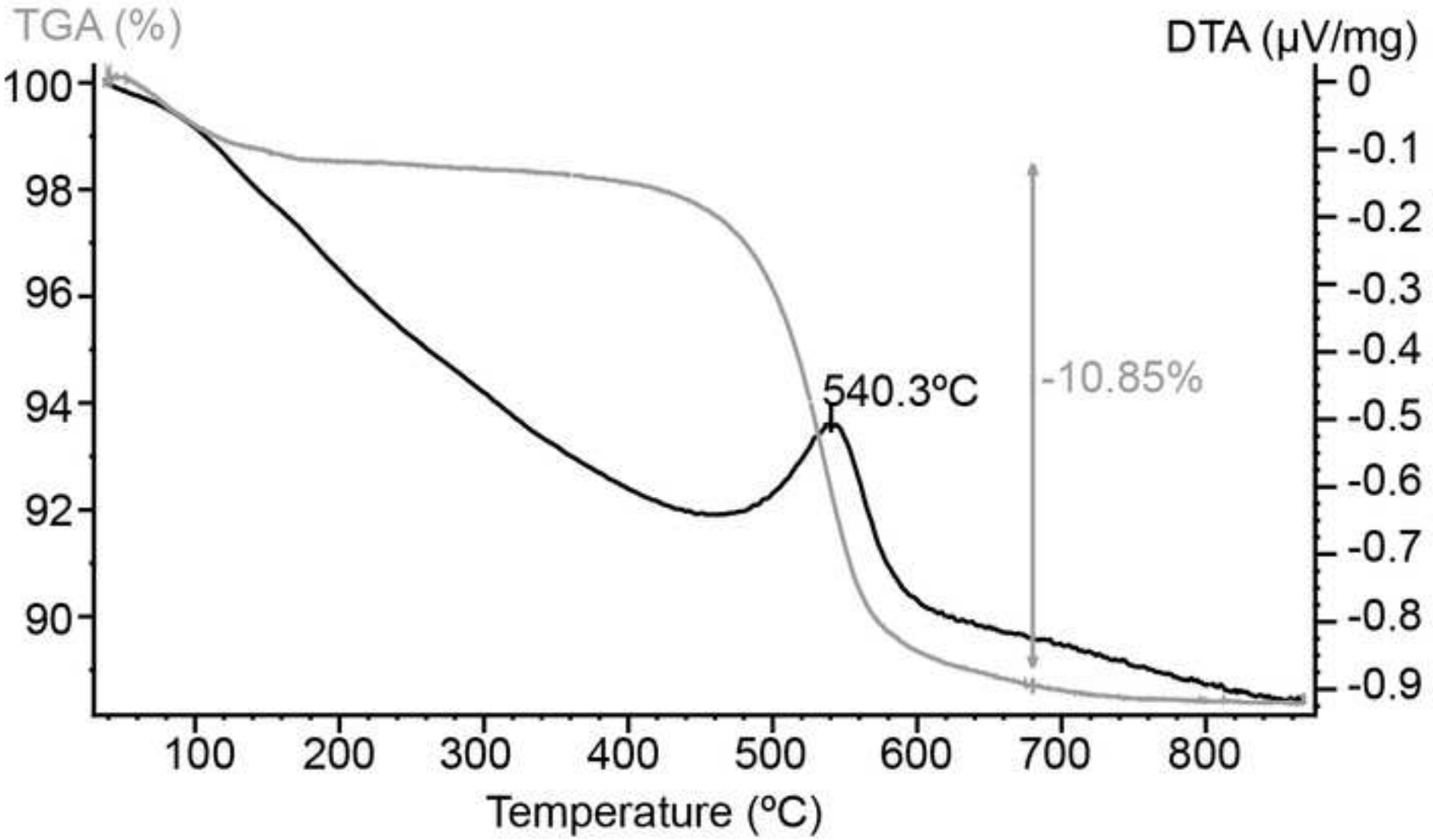

Figure 8

Click here to access/download;Figure;Fig_8.png

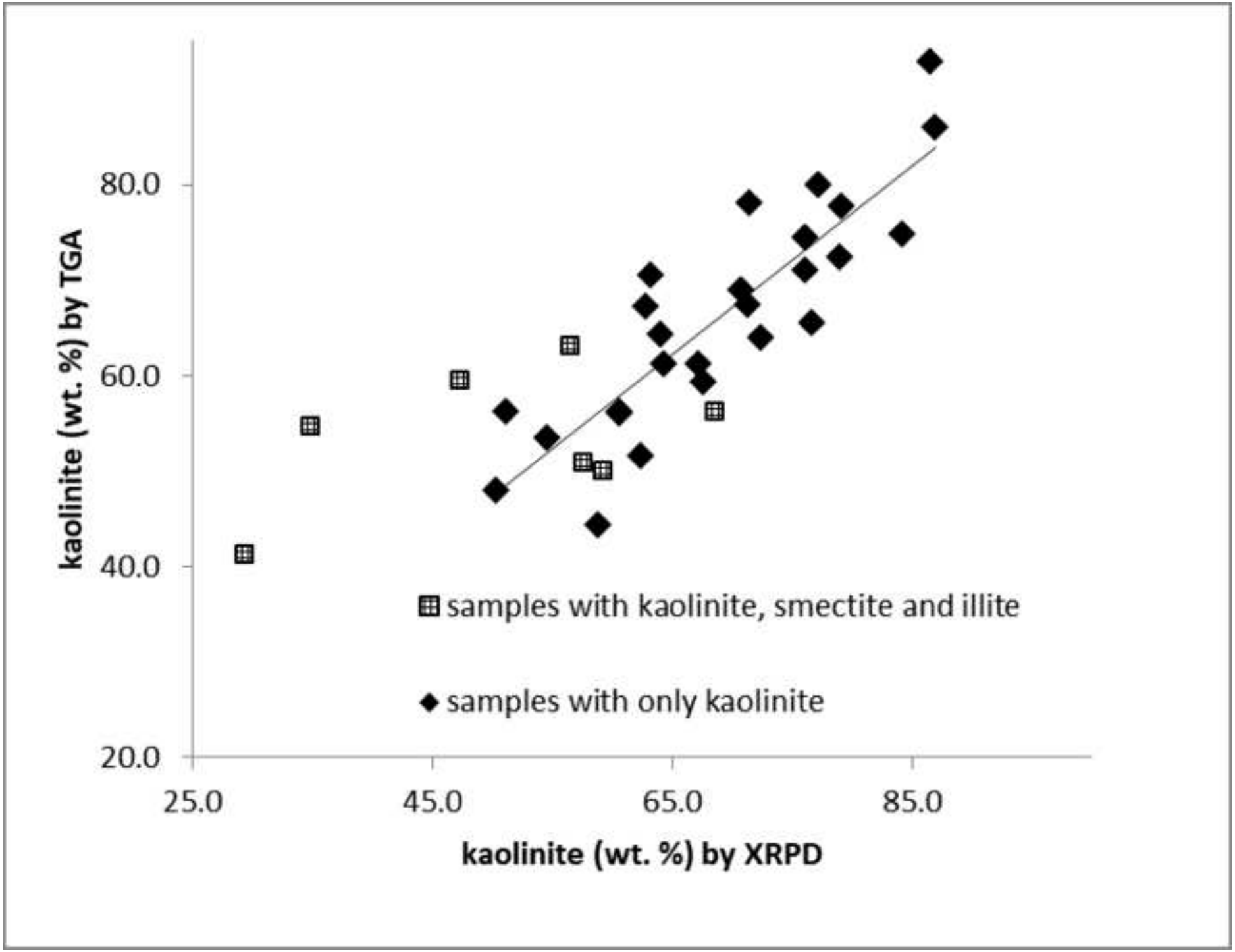

Figure 9

Click here to access/download;Figure;Fig_9jpg.jpg

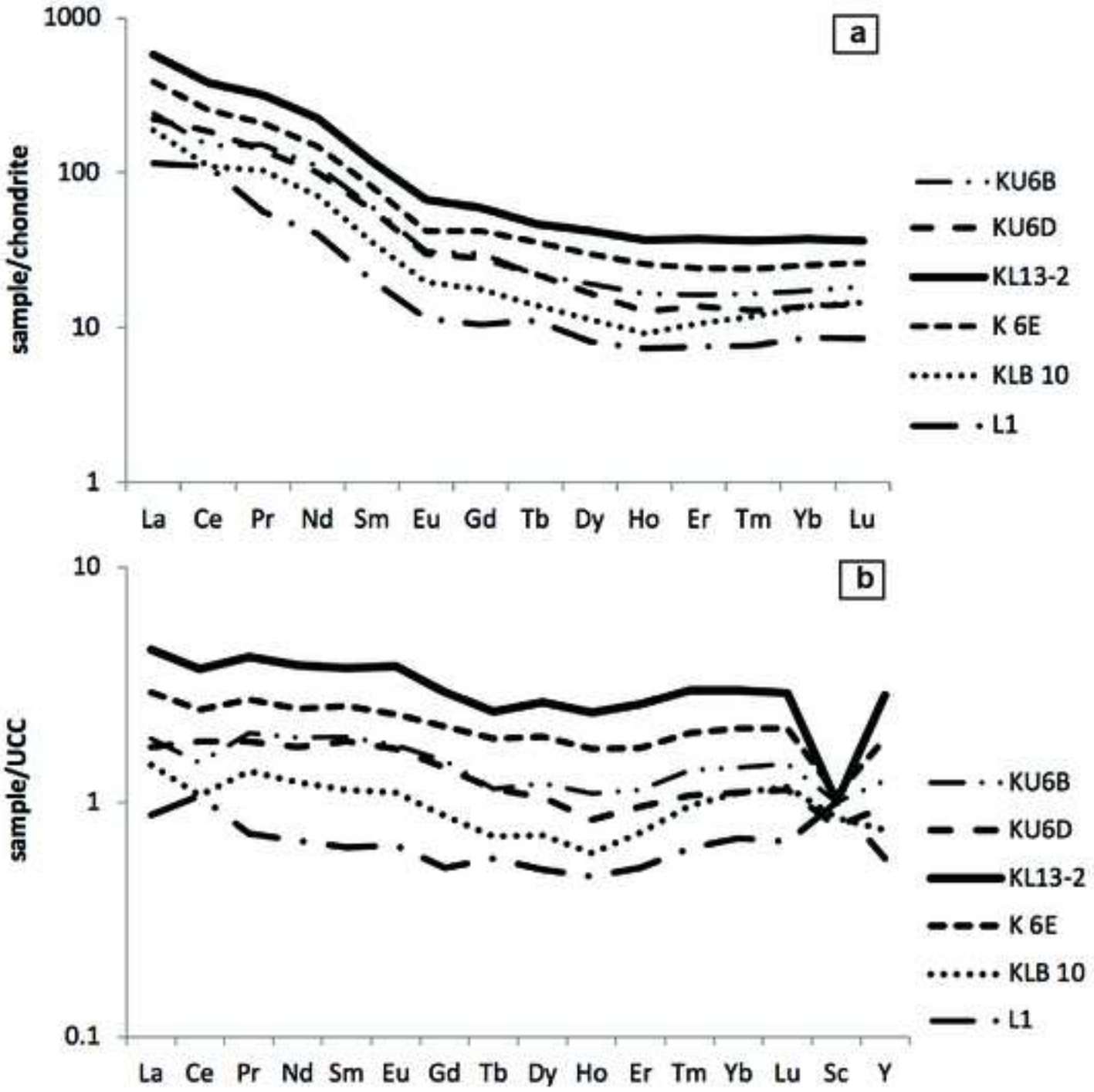

Table 1

Full profile refinement XRPD (wt. %)						
Sample	kaolinite	muscovite	quartz	plagioclase	microcline	hematite
KA	87	8.6	0.3	2	2.1	0.02
K6E	67.2	10.7	13.1	5.9	3	0.06
K10	64.3	17	10.1	5.3	3.2	0.05
KP1	70.8	8.5	2.8	1.97	11.9	1.6
KC12	50.4	21.3	23.5	3.8	0.9	0.07
KC5 C	51.2	27.3	11.5	7.4	2.6	0.04
KU3	79.2	1.1	14.8	2.9	1.4	0.58
KU6B	71.5	3.9	7.7	1.8	15.1	0
KU6D	58.9	5.5	10.5	3.6	21.5	0.04
KU8B	54.6	24.6	8.8	2.1	9.8	0.07
KRC3B	63.3	21.4	2.9	0.3	12.1	0.03
KRC5B	62.8	23.9	3.5	3.9	5.9	0.04
KRC5B1	64.1	20.8	4	4.6	6.5	0.03
KRY23	76.7	9.9	7.7	0.9	4.8	0.03
KRCA	77.3	8.4	5.7	4.5	4.1	0.04
KK14C	60.6	29.2	4.3	0.3	5.1	0.5
KKL13B	71.3	17.2	5.3	1.7	4.4	0.06
KKL17B	76.2	11.5	4.2	4	4.1	0.04
KL9	62.4	12.4	15.1	4.3	5.7	0.11
KL11	67.6	14.9	10.2	1.7	5.5	0.06
KL12A	76.2	11.2	4.8	4.7	3	0.06
KL13-2	84.2	2.9	0	5.7	6.7	0.5
KL14B	60.6	26	5.1	1.2	7.1	0.02
KL16B	72.4	15.4	5.3	2.6	4.1	0.2
L-1	86.6	3.9	1.9	6.3	1.2	0.1
L-2	79	7.3	6.9	3.2	3.6	0.01

Tm (ºC)	TGA Mass loss (wt.%)	kaolinite (wt. %)
550.3	12.0	85.9
531.0	8.6	61.1
529.3	8.6	61.1
539.1	9.7	68.9
518.7	6.7	47.9
530.4	7.9	56.2
526.6	10.9	77.6
531.4	10.9	78.0
520.0	6.2	44.3
530.1	7.5	53.4
542.4	9.9	70.4
540.8	9.4	67.2
541.0	9.0	64.3
532.3	9.2	65.5
546.0	11.2	80.0
528.3	7.9	56.2
534.2	9.4	67.4
541.8	10.4	74.4
525.4	7.2	51.5
537.6	8.3	59.2
536.0	10.0	71.0
540.3	10.5	74.8
541.6	7.8	56.0
537.2	9.0	64.0
527.9	13.0	92.9
518.4	10.1	72.4

Table 2

	Full profile refinement XRPD (wt.%)					
Sample	kaolinite	muscovite	illite	smectite	quartz	plagioclase
KK8	54	12	15		9	4
KK11A	57.6		8.1		5.7	2.1
KK13	59.3		7.4		9.6	2.8
KL6E	29.4	30.6		16.7	5.5	11.5
KL7B	56.5	9.9	18.4		3.8	4.8
KL8E*	34.8	23.8		15.8	4.8	6.0
KLB10	47.4	24.0		10.1	5.5	4.0
L-3	68.6	2.7	22.1		3.9	2.0

microcline	hematite	Tm (ºC)	TGA Mass loss (wt.%)	kaolinite (wt.%)
6	0	520.1	7.7	54.8
3.6	0.0	531.6	7.1	50.9
8.0	0.2	528.3	7.0	50.0
6.3	0.0	525.9	5.8	41.2
6.5	0.0	535.0	8.8	63.1
14.5	0.4	537.7	7.6	54.6
9.0	0.1	530.8	8.3	59.5
0.6	0.0	521.9	7.9	56.2

Table 3

Major elements wt.%	Caluquembe Angola KU6B	Caluquembe Angola KU6D	Caluquembe Angola KL13-2	Caluquembe Angola K 6E	Caluquembe Angola KLB 10
SiO_2	53.10	63.24	45.35	56.08	51.57
Al_2O_3	27.72	21.89	31.79	26.60	27.07
TiO_2	0.57	0.49	0.86	0.79	0.69
Fe_2O_3(T)	3.58	1.54	4.15	1.36	4.25
MnO	0.02	0.01	0.18	0.01	0.02
MgO	0.52	0.31	0.50	0.17	0.80
CaO	0.13	0.15	0.18	0.09	0.08
Na_2O	0.07	0.14	0.03	0.01	0.04
K_2O	3.55	4.03	2.02	1.16	3.63
P_2O_5	0.04	0.03	0.01	0.08	0.03
LOI	10.55	7.80	13.69	12.71	10.98
Total	99.84	99.64	98.74	99.07	99.17
CIA	87	82	93	95	87

Caluquembe Angola L1	Buwambo Uganda BW-1	Migade Uganda MG-1	Mayouom Cameroon sand-p MY03	Huambo Angola Sa Bandeira
48.76	49.98	49.90	46.61	72.21
32.24	35.97	35.62	33.29	15.02
0.62	0.02	0.05	3.96	0.40
2.75	0.34	0.54	1.46	0.29
0.02	0.05	0.04	< dl	0.06
0.52	0.33	0.34	< dl	0.80
0.06	<0.010	<0.01	< dl	2.37
0.01	0.03	0.04	< dl	3.23
1.65	0.99	0.78	0.94	3.86
0.01	0.06	0.11	0.40	0.08
12.48	12.61	12.85	13.97	1.00
99.13	100.35	100.23	99.87	100.50
92	97	97	97	52

Table 4

	Caluquembe	Caluquembe	Caluquembe	Caluquembe	Caluquembe	Caluquembe	Buwambo
	Angola	Angola	Angola	Angola	Angola	Angola	Uganda
ppm	KU6B	KU6D	KL13-2	K 6E	KLB 10	L1	BW-1
Be	4	3	3	3	3	4	n.d.
V	101	69	51	54	77	74	<15
Cr	< 20	< 20	< 20	30	< 20	20	4.47
Co	6	5	10	8	7	7	1.3
Ni	< 20	< 20	< 20	< 20	< 20	< 20	19
Cu	10	< 10	50	20	50	10	52
Zn	60	50	50	50	90	60	16
Ga	36	29	42	31	34	26	n.d.
Ge	2	2	2	2	2	2	n.d.
As	< 5	< 5	5	< 5	< 5	< 5	0.12
Rb	167	155	54	113	206	130	58.3
Sr	40	41	65	20	44	22	39.1
Zr	368	281	337	430	278	162	142
Nb	18	15	22	24	14	17	6
Mo	< 2	< 2	2	< 2	< 2	< 2	n.d.
Ag	1.3	1	1.3	1.5	1	< 0.5	n.d.
In	< 0.2	< 0.2	< 0.2	< 0.2	< 0.2	< 0.2	n.d.
Sn	3	2	4	4	5	3	n.d.
Sb	< 0.5	< 0.5	< 0.5	< 0.5	< 0.5	< 0.5	n.d.
Cs	3.3	3	< 0.5	5.9	2.4	3.9	2.27
Ba	595	683	1090	222	871	307	63.2
Bi	< 0.4	< 0.4	1.5	< 0.4	< 0.4	0.6	n.d.
Hf	9.8	7.5	8.7	10.7	6.9	4.9	0.66
Ta	1.8	1.7	2.3	3.1	1.7	1.6	0.34
W	5	3	13	6	6	4	n.d.
Tl	0.8	0.7	0.5	0.6	0.9	0.5	n.d.
Pb	36	36	40	38	22	26	n.d.
Th	25.1	20.1	48.6	31.7	16.9	17.9	1.66
U	7.1	6	5.6	17.2	16.1	5.9	0.84

Migade	Mayouom
Uganda	Cameroon
MG-1	sand-p MY03
n.d.	<dl
<15	718
10.9	294
1.75	1.8
24	5.4
105	n.d.
24	43.2
n.d.	38
n.d.	1.77
0.23	n.d.
58	17.3
65.9	383
139	489
6	57.9
n.d.	4.08
n.d.	n.d.
n.d.	0.18
n.d.	3.51
n.d.	n.d.
3.61	1.01
114	644
n.d.	n.d.
0.86	11.2
0.38	4.44
n.d.	0.8
n.d.	n.d.
n.d.	9.62
1.25	6.86
1	1.75

Table 5

ppm	Angola KU6B	Angola KU6D	Angola KL13-2	Angola K 6E	Angola KLB 10	Angola L1	Uganda BW-1	Uganda MG-1	Cameroon sand-p MY03
La	57.5	53.1	138	91.3	44.6	27.4	101	215	120
Ce	92.2	114	232	156	67	67	37.5	143	243
Pr	14	12.9	29.5	19.4	9.59	5.23	n.d.	n.d.	27.3
Nd	50.8	46.2	103	67.5	32.6	18.4	51.5	159	96.5
Sm	8.9	8.5	17.5	12.1	5.3	3	9.69	15.8	20.3
Eu	1.74	1.69	3.8	2.37	1.1	0.65	2.16	2.25	5
Gd	6	5.6	11.8	8.4	3.5	2.1	5.51	4.61	17.4
Tb	0.8	0.8	1.7	1.3	0.5	0.4	0.9	0.71	2.34
Dy	4.7	4.1	10.4	7.4	2.8	2	n.d.	n.d.	12.7
Ho	0.9	0.7	2	1.4	0.5	0.4	n.d.	n.d.	2.09
Er	2.6	2.2	6	3.9	1.7	1.2	n.d.	n.d.	4.86
Tm	0.41	0.32	0.9	0.59	0.29	0.19	0.26	0.29	0.7
Yb	2.8	2.2	6	4.1	2.2	1.4	1.21	1.03	4.1
Lu	0.45	0.35	0.9	0.64	0.36	0.21	0.14	0.1	0.6
Sc	14	11	14	15	12	14	1.2	1.89	0
Y	26	20	60	39	16	12	10	8	48.3
∑REE	243.8	252.66	563.5	376.4	172.04	129.58	209.87	541.79	556.89
∑LREE	225.14	236.39	523.8	348.67	160.19	121.68	201.85	535.05	512.1
∑HREE	18.66	16.27	39.7	27.73	11.85	7.9	8.02	6.74	44.79
LREE/HREE	12.07	14.53	13.19	12.57	13.52	15.40	25.17	79.38	11.43
La/Th	2.29	2.64	2.84	2.88	2.64	1.53	60.84	172.00	17.49
Y/HREE	1.39	1.23	1.51	1.41	1.35	1.52	1.25	1.19	1.08

UCC	C1Ch.
31	0.237
63	0.613
7.1	0.0928
27	0.457
4.7	0.148
1	0.0563
4	0.199
0.7	0.0361
3.9	0.246
0.83	0.0546
2.3	0.16
0.3	0.0247
2	0.161
0.31	0.0246
14	5.92
21	0.026

Table 6

	Caluquembe Angola whole rock granite	Mayouom western Cameroon sand-poor kaolin mylonite	Koutaba western Cameroon whole rock granite	Buwambo central Uganda whole rock granite	Migade Central Uganda whole rock granite	Mevaiela Angola <2 µm fraction anorthosite
kaolinite	50 to 87	76 to 85	32 to 51	82 to 94	84 to 91	≈ 100
quartz	0 to 23.5	2 to 9	32 to 52	0 to 10	5 to 10	detected
muscovite/illite	1 to 27	1 to 8	up to 12	3 to 6	3 to 5	detected
feldspars	2 to 21	n.d.	0 to 4	1 to 4	1 to 2	detected
anatase	n.d.	3.7 to 4	n.d.	n.d.	n.d.	n.d.
hematite/goethite	0 to 1.6	0.6 to 1.4	6 to 7	n.d.	n.d.	n.d.
pyrophilite	n.d.	n.d.	n.d.	n.d.	n.d.	n.d.
references	this work	Njoya et al., 2006	Nkalih Mefire et al., 2015	Nyakairu et al., 2001	Nyakairu et al., 2002	Saviano et al., 2005

Grahamstown South Africa Witteberg shale granite	Makoro southheastern Botswana whole rock arkose	Zhanjiang, Longyan, Guangdong province China granite	Otovice Czech Republic granite	Cornwall south-west England granite
20 to 70	major	96	82 to 92	81 to 93
30 to 60	minor	0 to 1	1 to 2	1 to 2
10 to 25	trace	3 to 4	4 to 16	4 to 15
5	trace	0	n.d.	n.d.
n.d.	n.d.	n.d.	n.d.	n.d.
n.d.	trace	n.d.	n.d.	n.d.
up to 35	n.d.	n.d.	n.d.	n.d.
Heckroodt, 1991	Ekosse, 2000	Wilson et al., 1997	Wilson and Jiranek, 1995	Wilson and Jiranek, 1995